

High-risk plaque features can be detected in non-stenotic carotid plaques of patients with ischaemic stroke classified as cryptogenic using combined ^{18}F -FDG PET/MR imaging

Fabien Hyafil^{1,2} · Andreas Schindler³ · Dominik Sepp⁴ · Tilman Obenhuber³ · Anna Bayer-Karpinska⁵ · Tobias Boeckh-Behrens⁶ · Sabine Höhn⁴ · Marcus Hacker⁷ · Stephan G. Nekolla^{1,8} · Axel Rominger⁹ · Martin Dichgans^{4,10} · Markus Schwaiger¹ · Tobias Saam³ · Holger Poppert⁴

Received: 18 June 2015 / Accepted: 17 September 2015 / Published online: 3 October 2015
© Springer-Verlag Berlin Heidelberg 2015

Abstract

Purpose The aim of this study was to investigate in 18 patients with ischaemic stroke classified as cryptogenic and presenting non-stenotic carotid atherosclerotic plaques the morphological and biological aspects of these plaques with magnetic resonance imaging (MRI) and ^{18}F -fluoro-deoxyglucose positron emission tomography (^{18}F -FDG PET) imaging.

Methods Carotid arteries were imaged 150 min after injection of ^{18}F -FDG with a combined PET/MRI system. American Heart Association (AHA) lesion type and plaque composition were determined on consecutive MRI axial sections ($n=460$) in both carotid arteries. ^{18}F -FDG uptake in carotid arteries was quantified using tissue to background ratio (TBR) on corresponding PET sections.

Results The prevalence of complicated atherosclerotic plaques (AHA lesion type VI) detected with high-resolution MRI was

significantly higher in the carotid artery ipsilateral to the ischaemic stroke as compared to the contralateral side (39 vs 0 %; $p=0.001$). For all other AHA lesion types, no significant differences were found between ipsilateral and contralateral sides. In addition, atherosclerotic plaques classified as high-risk lesions with MRI (AHA lesion type VI) were associated with higher ^{18}F -FDG uptake in comparison with other AHA lesions (TBR=3.43±1.13 vs 2.41±0.84, respectively; $p<0.001$). Furthermore, patients presenting at least one complicated lesion (AHA lesion type VI) with MRI showed significantly higher ^{18}F -FDG uptake in both carotid arteries (ipsilateral and contralateral to the stroke) in comparison with carotid arteries of patients showing no complicated lesion with MRI (mean TBR=3.18±1.26 and 2.80±0.94 vs 2.19±0.57, respectively; $p<0.05$) in favour of a diffuse inflammatory process along both carotid arteries associated with complicated plaques.

Fabien Hyafil and Andreas Schindler contributed equally to this work.

✉ Fabien Hyafil
fabien.hyafil@gmail.com

¹ Department of Nuclear Medicine, Klinikum rechts der Isar, Technische Universität München, Munich, Germany

² Department of Nuclear Medicine, Bichat University Hospital, Inserm 1148, DHU FIRE, Assistance Publique – Hôpitaux de Paris, Paris, France

³ Institute for Clinical Radiology, Ludwig Maximilians University Hospital Munich, Munich, Germany

⁴ Department of Neurology, Klinikum rechts der Isar, Technische Universität München, Munich, Germany

⁵ Institute for Stroke and Dementia Research, Ludwig Maximilians University Hospital Munich, Munich, Germany

⁶ Department of Neuroradiology, Klinikum Rechts der Isar, Technische Universität München, Munich, Germany

⁷ Division of Nuclear Medicine, Department of Biomedical Imaging and Image-guided Therapy, Medical University of Vienna, Vienna, Austria

⁸ German Centre for Cardiovascular Research (DZHK), Partner Site Munich Heart Alliance, Munich, Germany

⁹ Department of Nuclear Medicine, Ludwig Maximilians University Hospital Munich, Munich, Germany

¹⁰ Munich Cluster of Systems Neurology (SyNergy), Munich, Germany

Conclusion Morphological and biological features of high-risk plaques can be detected with ^{18}F -FDG PET/MRI in non-stenotic atherosclerotic plaques ipsilateral to the stroke, suggesting a causal role for these plaques in stroke. Combined ^{18}F -FDG PET/MRI systems might help in the evaluation of patients with ischaemic stroke classified as cryptogenic.

Keywords Atherosclerosis · Vulnerable plaque · Carotid arteries · Stroke · MRI · PET · ^{18}F -FDG

Introduction

Stroke is one of the leading causes of death and handicap in industrialized countries [1, 2]. Carotid plaques are estimated to cause between 15 and 20 % of all ischaemic strokes [3, 4]. Plaque rupture is identified in about 60 % of endarterectomy specimens of patients presenting with ischaemic stroke and is thought to represent a key trigger for arterial thromboembolism [5]. However, diagnostic and therapeutic strategies in patients with carotid stenosis remain based on the degree of luminal stenosis and the presence of acute ischaemia in the downstream cerebral vascular territory [6]. Detection of ruptured plaque with noninvasive imaging might help us to identify the cause of stroke or intermittent cerebral ischaemia in symptomatic patients and to improve risk stratification in patients with asymptomatic carotid stenosis.

In the past 20 years, several noninvasive imaging techniques have emerged for the characterization of carotid atherosclerotic plaques [7, 8]. Morphological plaque features such as thin/ruptured fibrous cap, large lipid-rich/necrotic core (LR/NC) or intraplaque haemorrhage (IPH) are characteristic of the so-called vulnerable plaque and can be detected by high-resolution magnetic resonance imaging (MRI) with good accuracy in comparison with histology [9, 10]. Additionally, carotid plaques of patients with recent ischaemic stroke contain high numbers of inflammatory cells, which can be evidenced using ^{18}F -fluorodeoxyglucose (FDG), a glucose analogue radiolabelled for positron emission tomography (PET) imaging that accumulates in metabolically active cells such as activated macrophages. Strong relationships have been documented between the degree of arterial ^{18}F -FDG uptake and the density of macrophages determined histologically in carotid plaques [11]. Moreover, atherosclerotic plaques of patients with carotid stenosis >50 % imaged shortly after a transient ischaemic attack accumulated approximately 30 % more ^{18}F -FDG in carotid arteries ipsilateral to the stroke than in contralateral arteries [12]. Combined PET/MRI imaging systems [13] have recently become available and might prove particularly interesting for vascular imaging by offering simultaneous morphological and functional evaluation of atherosclerotic plaques [14].

Non-stenotic carotid plaques represent a promising clinical application for plaque imaging. Indeed, in up to 40 % of patients presenting with ischaemic stroke despite extensive work-up, no definite cause can be established [15]. In a first pilot study [16], we imaged patients admitted for an ischaemic stroke considered as cryptogenic and presenting non-stenotic carotid atherosclerotic plaques ipsilateral to the stroke with multi-contrast MRI. We found that about one third of carotid plaques were complicated by IPH, fibrous plaque rupture or luminal thrombus [American Heart Association (AHA) lesion type VI]. Accurate identification of culprit atherosclerotic plaques associated with ischaemic stroke is crucial because the prevalence of carotid stenosis <50 % is high in the population. Histological analysis of plaques is, however, not available in these patients because most of the time they are treated medically. In the current study, we exploited the methodological opportunity of PET/MRI to simultaneously evaluate the morphological and functional features of atherosclerotic plaques in non-stenotic carotid lesions of a subgroup of 18 symptomatic patients included in the Carotid Plaque Imaging in Acute Stroke (CAPIAS) study (NCT01284933) [17].

Materials and methods

Patient selection

Eighteen consecutive patients admitted to the stroke unit of the Department of Neurology of the University Hospital Klinikum rechts der Isar in Munich, Germany, between December 2012 and March 2014 were included in the CAPIAS study on the basis of previously published inclusion and exclusion criteria [17]. Briefly, patients were screened for eligibility in the study on the basis of ischaemic stroke in the territory of the anterior or middle cerebral artery <14 days, non-stenosing atherosclerotic plaques in the carotid bifurcation determined by duplex sonography [plaque thickness > 2 mm; luminal stenosis <50 % according to North American Symptomatic Carotid Endarterectomy Trial (NASCET) criteria] and absence of any definite stroke aetiology. The local Ethics Committee approved the study and all participants provided written informed consent.

Acquisition protocols with the combined PET/MRI system

PET and MR images were acquired simultaneously in all patients.

FDG PET acquisition protocol

All patients were asked to fast for at least 6 h before ^{18}F -FDG PET imaging. Imaging was performed only if fasting glucose was lower than 7.7 mmol/l before tracer injection. ^{18}F -FDG

was injected intravenously at a dose of 4 MBq/kg and patients were hydrated orally with water. The patient's neck was placed in a support device on the examination table and covered with dedicated carotid MRI coils. Imaging started 150 ± 14 min after tracer injection on a fully integrated whole-body PET/MRI scanner (Biograph mMR, Siemens Healthcare). The imaging protocol consisted of a localizer scan to define the bed position and was followed by a coronal two-point Dixon 3-D T1-weighted (T1W) volumetric interpolated breath-hold (VIBE) MRI sequence for the generation of attenuation maps (μ -maps) as previously described [18]. The field of view for PET acquisition was centred on the carotid bifurcations, identified by time-of-flight (TOF) MR angiography. PET was then acquired in 3-D mode for 10 min in a single bed position. Data were corrected for randoms, dead time, scatter and attenuation based on the μ -maps extracted from the Dixon images. Using a 3-D attenuation-weighted ordered subsets expectation maximization iterative reconstruction algorithm (AW-OSEM 3-D) with 3 iterations and 21 subsets and a zoom of 1, 2-mm-thick axial PET images were reconstructed with a 50×50 cm² field of view and a 344×344 matrix. Spatial resolution of the reconstructed PET images was previously determined to be 4.3 mm at 1 cm from the scanner's isocentre and 5.0 mm at 10 cm in the transverse direction in full-width at half-maximum [19]. Total radiation dose for the PET acquisition was estimated at 5 mSv [20].

MRI acquisition protocol

All subjects were imaged using a previously published multiple sequence protocol [21] [3-D TOF MR angiography, axial fat suppressed pre- and post-contrast black-blood T1W and T2-weighted (T2W) sequences; in-plane resolution 0.5×0.5 mm² with the 3-T MRI system]. A dedicated bilateral four-channel phased array carotid coil (PACC-ST30, Machnet, The Netherlands) was used to improve the signal to noise ratio and to optimize spatial resolution of MR images. Sequences were centred to depict both carotid bifurcations with adjacent sections of common and internal carotid arteries. Parallel imaging was used for all sequences with a parallel acquisition technique (PAT) acceleration factor of 2. Imaging times for TOF, T1W and T2W images were 3.00, 4.50 and 2.26 min, respectively, resulting in a total scan time of 15.06 min. Gadolinium-DTPA-BMA (gadobutrol, Bayer Schering, Leverkusen, Germany) of 0.1 mmol/kg (0.1 ml/kg) was given at a rate of 3 ml/s. Post-contrast T1W imaging was performed approximately 5 min after intravenous injection of the contrast agent. Scan coverage was 3.0, 4.2 and 5.2 cm for T1W, T2W and TOF images, respectively, resulting in a matched coverage of 30 mm (2-mm slice thickness \times 15 matched images across the three sequences).

Analysis of FDG PET images

Images were analysed by an experienced nuclear medicine physician (F.H.) blinded to clinical status and to the results of MRI. Image registration and fusion of the TOF MRI acquisitions and attenuation-corrected PET images was performed with an OsiriX workstation (OsiriX version 3.5.1 64-bit, OsiriX Imaging Software, Geneva, Switzerland), an open-source DICOM viewer and image manipulator using the Horn algorithm, a manual rigid registration algorithm based on multiple points [22, 23]. Matching of both data sets was considered as correct when neck contours of PET and MR images were perfectly aligned. If required, alignment was corrected manually using the fusion tool of the OsiriX software. Circular regions of interest (ROIs) were then placed on axial adjacent PET images of both carotid arteries (15 axial sections) identified using the TOF images. Care was taken to exclude FDG uptake located in adjacent lymph nodes. Maximum standard uptake values (SUV_{max}) calculated as decay-corrected tissue radioactivity divided by body weight and injected dose were recorded in each region of interest. Tissue to background ratio (TBR) was calculated as the ratio of SUV_{max} and the background venous activity measured as SUV_{mean} in the internal jugular veins [24]. In addition, mean TBRs for each arterial territory were calculated as the average of TBR values throughout the entire segment of the carotid artery present in the field of view.

Analysis of MR images of atherosclerotic plaques

MRI data were independently analysed by two experienced radiologists (T.S. and A.S.) who were blinded to the clinical status and to the results of PET scans. In cases of discrepancy, a consensus decision was made. Image quality was assessed on a 4-point Likert scale (1=worst; 4=best) and only images with a value ≥ 2 were included for further evaluation. Atherosclerotic plaques in both carotid arteries were analysed and classified per slice according to the modified criteria of the AHA [25]. Area measurements of the lumen, wall, outer wall and tissue components were obtained using a custom-designed semiautomatic image analysis tool (CASCADE, University of Washington, Seattle, WA, USA) [26]. Tissue components (LR/NC, calcification and haemorrhage), the status of the fibrous cap (thick vs thin vs ruptured), haemorrhage type [type I (early subacute) versus type II (late subacute)] and presence of thrombus were identified on the basis of previously published criteria [27–29].

Statistical analysis

Categorical variables are presented as absolute and relative frequencies; continuous variables are presented as mean \pm SD. For comparisons of ipsilateral and contralateral carotid arteries, the

paired Student's *t* test was used to test differences between continuous variables and Fisher's exact test to determine differences between categorical variables. A two-sided Kruskal-Wallis test was used for comparisons of plaque composition in individual axial sections of carotid arteries. A Mann-Whitney test was used for comparison of the effects of statin therapy and imaging delay on TBR values. All analysis was performed using SAS version 9.2 (SAS Institute, Inc., Cary, NC, USA). A *p* value < 0.05 was considered statistically significant.

Results

Patient population

A total of 18 patients (mean age 70±12 years; 37 % male) with recent acute ischaemic stroke and ipsilateral non-stenotic carotid atherosclerotic plaques were included in the study. Despite detailed clinical work-up, no definite stroke aetiology was identified in any of these patients when they were included in this study. Demographic and clinical characteristics are described in Table 1. The mean modified National Institute of Health Stroke Scale (NIHSS) [30] score upon admission was 3.5±4.4. Median time between acute ischaemic stroke and imaging was 7±3 days. The average modified Rankin Scale and Barthel Index upon discharge was 1.7±1.2 and 92±14, respectively.

Morphology of carotid atherosclerotic plaques on multi-contrast MRI

A total of 460 of 540 (85.2 %) axial MR image sections were deemed interpretable. None of the patients had to be excluded

Table 1 Patient population

	<i>n</i>	%
Vascular risk factors/comorbidities		
Active smoking	3	17
Former smoking	10	56
Diabetes mellitus	4	22
Hypercholesterolaemia	5	28
Arterial hypertension	13	72
Positive family history for vascular events	10	56
Overweight (body mass index > 25 kg/m ²)	12	67
Coronary artery disease	4	22
Peripheral arterial disease	2	11
Baseline medication		
Antiplatelet agent plus statin	4	22
Statin only	2	11
Antiplatelet agent only	3	17
Neither antiplatelet agent nor statin	9	50

due to poor image quality on MRI. Quantitative analysis of plaque burden and composition (Table 2) identified no significant differences for mean luminal area or mean total vessel area between both carotid arteries. By contrast, significantly larger maximal wall areas were measured in the carotid artery ipsilateral to the stroke as compared with the contralateral artery. In addition, ipsilateral carotid arteries showed significantly larger maximum necrotic core and maximum haemorrhagic areas than contralateral arteries. Maximum calcification areas did, however, not differ between ipsilateral and contralateral arteries.

Complicated atherosclerotic plaques (AHA type VI lesions) were detected in 39 % of carotid arteries ipsilateral to the ischaemic stroke (Table 2); by contrast, there were no AHA type VI plaques on the contralateral side (*p*=0.001). For all other AHA lesion types, no significant differences were found between the ipsilateral and contralateral sides. The most common feature of AHA type VI lesions was IPH (100 %), followed by fibrous plaque rupture (86 %) and luminal thrombus (14 %). Of the seven atherosclerotic plaques with IPH, one haemorrhage was classified as type I, and six were classified as type II.

¹⁸F-FDG uptake in carotid arteries measured with PET

Increased ¹⁸F-FDG uptake was measured in ruptured atherosclerotic plaques and in plaques with a thin fibrous cap with MRI as compared with non-ruptured lesions with thick fibrous caps (Fig. 1; TBR=3.55±1.21 and 3.14±1.05 vs 2.38±0.83, respectively; *p*<0.001). In addition, atherosclerotic plaques containing LR/NC or IPH with MRI (Fig. 2) showed significantly higher ¹⁸F-FDG uptake as compared with other lesions (3.14±1.14 vs 2.36±0.80 for the presence of an LR/NC; 3.48±1.11 vs 2.40±0.84 for the presence of IPH; *p*<0.001 each). Furthermore, plaques with large (≥5 mm²) as compared with small (<5 mm²) LR/NC were associated with higher ¹⁸F-FDG uptake (3.09±1.04 vs 2.58±1.05, respectively; *p*=0.001). Similarly, there was a strong trend for increased ¹⁸F-FDG uptake in plaques with large (≥5 mm²) as compared with small (<5 mm²) IPH type II, but this did not reach significance (3.76±1.05 vs 2.96±0.71, respectively; *p*=0.07). Atherosclerotic plaques classified as high-risk lesions with MRI (AHA lesions type VI) were associated with higher ¹⁸F-FDG uptake in comparison with other AHA lesions (TBR=3.43±1.13 vs 2.41±0.84; respectively; *p*<0.001).

Significantly higher ¹⁸F-FDG uptake (Fig. 3) was measured in both carotid arteries of patients presenting with complicated lesions with MRI in comparison with carotid arteries of patients showing no complicated lesion (Fig. 4; mean TBR=3.18±1.26 and 2.80±0.94 vs 2.19±0.57; *p*<0.05, respectively). No significant difference in ¹⁸F-FDG uptake was found between patients treated with statins vs untreated (mean TBR=2.33±0.60 vs 2.63±0.94; *p*=0.55, respectively) as well

Table 2 Plaque characteristics with MRI ipsilateral and contralateral to the vascular territory of ischaemic stroke

	Ipsilateral side (n=18)	Contralateral side (n=18)	p value
Plaque burden			
Mean total vessel area (mm ²)	58.1	55.9	0.34
Mean luminal area (mm ²)	28.7	31.5	0.33
Maximal wall area (mm ²)	47.8	37.2	0.003
Plaque composition (mm ²)			
Maximal lipid core area	11.3	1.6	<0.001
Maximal haemorrhagic area	0.5	0.0	0.02
Maximal calcified area	0.6	1.2	0.21
AHA lesion type distribution			
Type VI	7 (39 %)	0 (0 %)	0.008
IPH	7 (39 %)	0 (0 %)	0.008
Fibrous cap rupture	6 (33 %)	0 (0 %)	0.002
Thrombus	1 (6 %)	0 (0 %)	1
Type I	2 (11 %)	2 (11 %)	1
Type III	4 (22 %)	8 (44 %)	0.31
Type IV/V	2 (11 %)	3 (17 %)	0.63
Thin fibrous cap	1 (6 %)	0 (0 %)	1
Thick fibrous cap	1 (6 %)	3 (17 %)	0.60
Type VI	7 (39 %)	0 (0 %)	0.008
Type VII	3 (17 %)	5 (28 %)	0.69
Type VIII	0 (0 %)	0 (0 %)	1

as between patients imaged early (≤ 7 days) vs late (≥ 7 days) after the onset of symptoms (mean TBR = 2.50 ± 0.95 vs 2.51 ± 0.75 ; $p = 0.49$, respectively).

Discussion

In this study, we evaluated in 18 consecutive patients with ischaemic stroke classified as cryptogenic and presenting non-stenotic (<50 %) carotid atherosclerotic plaques the morphological and biological aspects of these plaques using a combined PET/MRI system. We found that the prevalence of morphological features of high-risk atherosclerotic plaques on MRI was significantly higher in the carotid artery ipsilateral to the stroke than in the contralateral artery. Non-stenotic, complicated plaques identified with MRI were associated with high levels of ¹⁸F-FDG uptake with PET. These observations highlight the value of combined PET/MRI systems for the simultaneous evaluation of morphological and functional characteristics of atherosclerotic plaques in carotid arteries and the more specific identification of high-risk plaques.

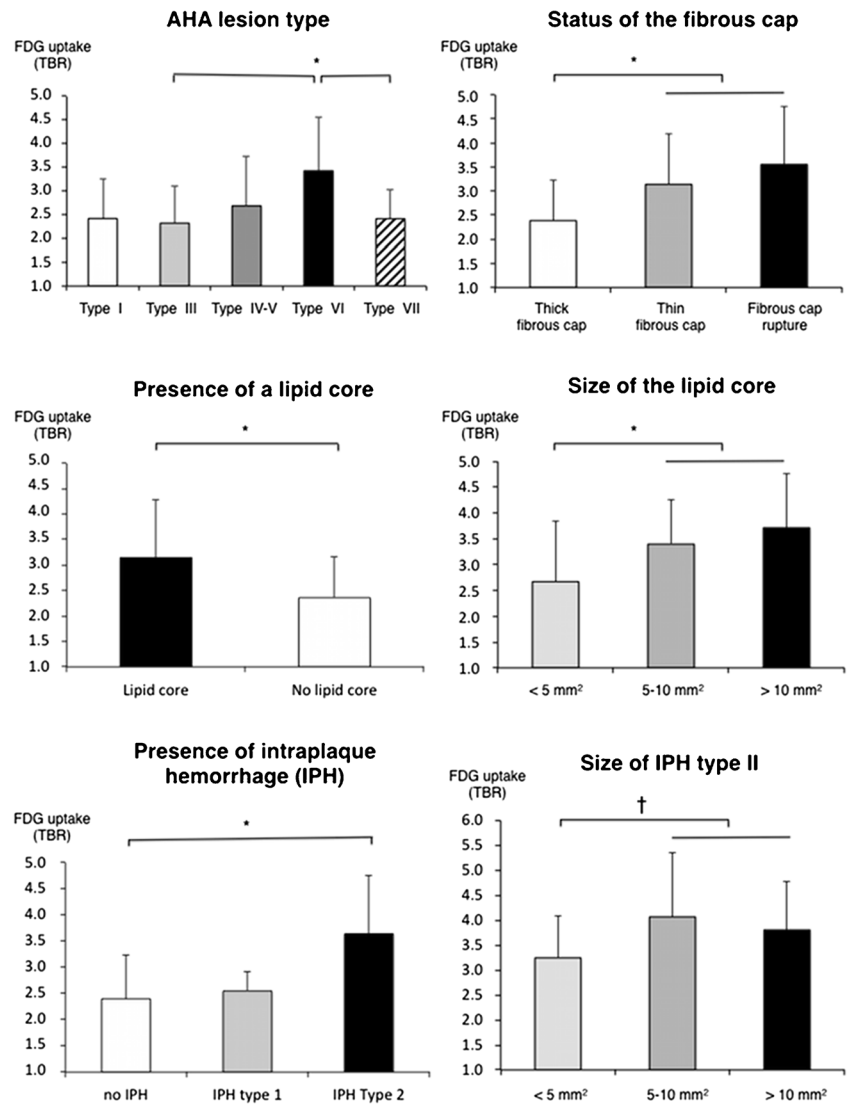
Association between morphological and functional aspects of high-risk plaques

In this study, we took advantage of simultaneous acquisition of high-resolution MRI and ¹⁸F-FDG PET imaging to

compare the morphological and functional characteristics of non-stenotic carotid plaques. The relationship between characteristics of carotid plaques with MRI and the intensity of ¹⁸F-FDG uptake has been previously evaluated in patients with high-grade carotid stenosis in two separate imaging sessions [31, 32]. High ¹⁸F-FDG uptake in carotid arteries was associated with the presence of lipid-rich carotid plaques detected with MRI as well as histologically. Plaque aspects with computed tomography angiography (CTA) have also been compared with the intensity of ¹⁸F-FDG uptake in patients with carotid stenosis >50 % [33]. A strong association was found between high-risk features of plaques identified with CTA and the intensity of ¹⁸F-FDG uptake. Characterization of plaques with CTA is, however, restricted to the detection of surface irregularities and areas of hypodensities. In addition, evaluation of non-stenotic plaques is often difficult with CTA owing to the poor contrast between plaque and lumen and the small size of these lesions.

In contrast, high-resolution MRI seems particularly well suited for the characterization of morphological aspects of non-stenotic lesions. Combined PET/MRI acquisitions also proved very helpful for the analysis of ¹⁸F-FDG PET images of carotid arteries, even though this point was not specifically evaluated in the current study. The high tissular contrast of MRI allowed us to identify more specifically the ¹⁸F-FDG signal located in the vessel wall and to exclude perivascular structures such as lymph nodes from analysis. In this study, we

Fig. 1 Relationship between morphological features of high-risk atherosclerotic plaques with MRI and the intensity of ^{18}F -FDG uptake with PET. Significantly higher ^{18}F -FDG uptake was measured in ruptured atherosclerotic plaques or in plaques with a thin fibrous cap on MRI as compared with other lesions. In addition, atherosclerotic plaques containing LR/NC or IPH with MRI showed significantly higher ^{18}F -FDG uptake as compared with lesions lacking these morphological features. Furthermore, plaques with large ($\geq 5\text{ mm}^2$) as compared with small ($< 5\text{ mm}^2$) LR/NC were associated with higher ^{18}F -FDG uptake. Similarly, there was a strong trend for increased ^{18}F -FDG uptake in plaques with large ($\geq 5\text{ mm}^2$) as compared with small ($< 5\text{ mm}^2$) IPH type II, but this did not reach significance. Furthermore, atherosclerotic plaques classified as high-risk on MRI (AHA lesions type VI) were associated with higher ^{18}F -FDG uptake in comparison with other AHA lesions. * $p < 0.05$; † $p = 0.07$



confirmed the strong association between morphological features of high-risk plaques with MRI and intense ^{18}F -FDG uptake with PET in patients with non-stenotic carotid plaques. In addition, we found that, in up to 40 % of patients presenting with ischaemic stroke classified as cryptogenic, non-stenotic plaques ipsilateral to the stroke present features of high-risk plaques with MRI and ^{18}F -FDG PET. These results suggest that combined ^{18}F -FDG PET/MRI might find a role in the evaluation of non-stenotic plaques in patients presenting with ischaemic stroke.

Diffuse ^{18}F -FDG uptake in carotid arteries of patients with complicated plaques

In this study, high uptake was detected in complicated non-stenotic carotid plaques but was also identified at slightly lower levels, along the carotid artery contralateral to the cerebral

territory of the stroke. This finding is in line with previous imaging studies performed in patients with stenotic carotid plaques [34]. Carotid arteries of patients presenting with recent ischaemic stroke were imaged with MRI after injection of ultrasmall superparamagnetic iron oxide nanoparticles (USPIO), which are phagocytosed by macrophages in plaques. USPIO accumulated in atherosclerotic plaques present in both carotid arteries (ipsilateral and contralateral to the territory of the stroke), whereas no significant USPIO uptake was detected in carotid arteries of asymptomatic patients. Similarly, Kwee et al. [35] found only a moderate difference in ^{18}F -FDG uptake between the carotid artery ipsilateral vs contralateral to the stroke in patients imaged within 38 days after ischaemic symptoms, whereas no significant difference could be found at later time points. Taken together, these results suggest that, in addition to the high ^{18}F -FDG uptake identified in complicated plaques, moderate ^{18}F -FDG uptake can be

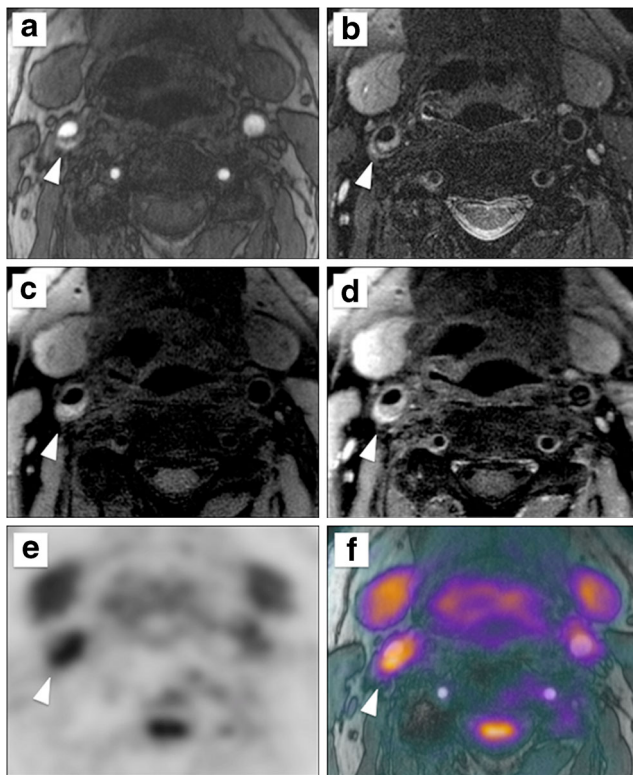


Fig. 2 Representative example of high-risk carotid atherosclerotic plaque formed of LR/NC and IPH imaged with combined ^{18}F -FDG PET/MRI. Corresponding axial views of non-stenotic carotid atherosclerotic plaque acquired simultaneously using a combined imaging system including MRI with successive high-resolution black-blood T2W (a), black-blood T1W before (b) and 5 min after injection of gadolinium chelates (c) and TOF sequences (d) and PET images (e) acquired 150 min after injection of ^{18}F -FDG allowing for perfect matching of both acquisitions (f; fusion image formed of TOF and ^{18}F -FDG PET images). Note the presence of a non-stenotic atherosclerotic plaque ipsilateral to the vascular territory of the stroke (a–d; white arrowheads) formed of a hypointense area on T1W, and T2W and TOF sequences and a hyperintense area on T1W, T2W and TOF sequences consistent with the presence of LR/NC associated with IPH type II. High accumulation of ^{18}F -FDG was detected with PET in the corresponding area (e–f; white arrowheads), supporting the presence of high inflammatory activity in the atherosclerotic plaque

detected along both carotid arteries, suggesting a diffuse inflammatory process in the vessels of these patients. This observation might explain why only weak correlations were previously measured between CT and MRI with respect to morphological features of high-risk plaques and the intensity of ^{18}F -FDG uptake in symptomatic patients [36].

Incremental value of ^{18}F -FDG PET over high-resolution MRI

An important diagnostic question remains concerning what the incremental role of ^{18}F -FDG PET over high-resolution MRI might be for the evaluation of non-stenotic atherosclerotic plaques, since features of high-risk plaques identified with each of these imaging

techniques were found in this study to be closely associated [37]. Interestingly, both the number of inflammatory cells measured on histology [38] and the intensity of ^{18}F -FDG uptake detected with PET [39] in atherosclerotic plaques have recently been shown to be independent predictors of early stroke recurrence in patients with carotid stenosis >50 %. In a similar way, we postulate that ^{18}F -FDG PET might, in addition to MRI, improve risk stratification of symptomatic patients with non-stenotic plaques and help to identify patients who may benefit from early interventional approaches. This hypothesis will need to be evaluated prospectively in a larger group of patients.

Limitations

This study has several reservations. First, the results of the present study are limited by the modest sample size, but its strength lies in the highly selected group of patients presenting with ischaemic stroke of unknown origin and non-stenotic carotid plaques included in the study. The absence of any alternative cause of ischaemic stroke in this group of patients strengthens the relationship observed between non-stenotic carotid plaques and ischaemic stroke. Second, PET axial sections were reconstructed with a slice thickness of 2 mm to allow for optimal matching with MR images. The true spatial resolution of PET images is in the range 4–5 mm. The intensity of ^{18}F -FDG uptake measured on each axial section with PET might therefore be partly influenced by signals originating from adjacent sections of atherosclerotic plaques. Third, important partial volume effects (PVE) occur in small structures such as the vascular wall which are less than three times the spatial resolution of reconstructed PET images and cause large underestimation of activities [40]. The metrics used for the quantification of FDG in this work, TBR, provides only an estimate of the absolute FDG signal present in plaques but has been formerly demonstrated to correlate with the degree of macrophage infiltration in carotid plaques [11]. Development of algorithms for PVE correction of PET acquisitions based on the morphology of plaques detected with MRI might help to improve the accuracy of FDG measurements in atherosclerotic plaques. Fourth, the MRI surface coils required for high-resolution plaque imaging cause an approximately 10 % attenuation of the PET signal [41]. Nevertheless, FDG uptake was quantified in this study using a ratio between SUVs measured in the carotid artery and in the jugular vein (TBR), both regions very similarly affected by the surface coils. Thus, quantification of FDG uptake in carotid plaques using TBR limits the effects of signal attenuation by coils. Furthermore, integrating the attenuation properties

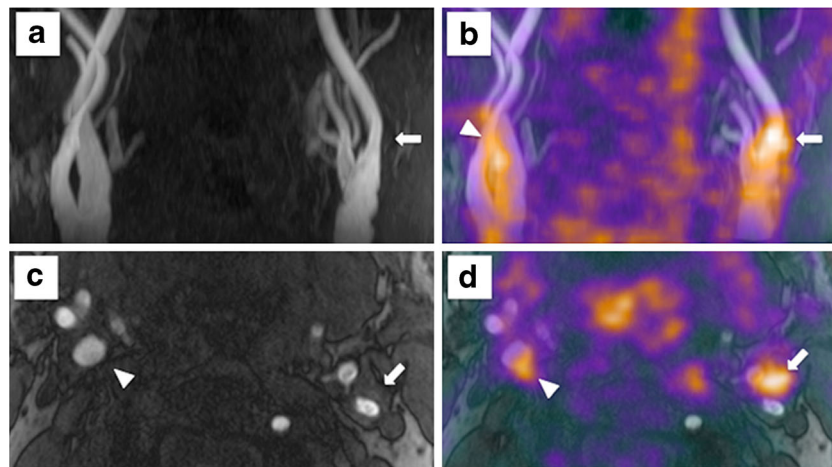


Fig. 3 Representative example of a non-stenotic plaque of the left carotid artery imaged with combined ^{18}F -FDG PET/MRI. Note the presence of a 40 % stenosis of the internal left carotid artery (NASCET criteria) ipsilateral to the territory of stroke on 3-D maximum intensity reconstruction of carotid arteries obtained from the TOF MRI acquisition (a). On the fused coronal images of PET and TOF MR angiography acquisitions (b), ^{18}F -FDG uptake was intense in the vascular wall of the left carotid artery (b, white arrow), but was also increased in the right carotid artery

contralateral to the stroke (b, white arrowhead). A large non-stenotic atherosclerotic plaque could be detected on axial views of TOF acquisition (c) at the origin of the left internal carotid artery (c, white arrow), whereas only a small plaque was present in the right carotid artery (c, white arrowhead). On the fused axial images of PET and TOF MR angiography acquisitions (b), high ^{18}F -FDG uptake could be detected in the vascular wall of both carotid arteries

of the surface coils into the map used for attenuation correction of PET images should help to overcome this current limitation of carotid plaque imaging with PET/MRI [42]. Finally, the characterization of carotid plaque morphology relied on in vivo MRI and no histological validation was available in these patients. Nevertheless, black-blood MRI has been formerly extensively validated against histopathology with excellent sensitivity and

specificity. Small haemorrhages, thrombi or fibrous cap ruptures might, however, have been missed in some of these plaques.

Conclusion

This work demonstrates that morphological and biological characteristics of plaques can be evaluated in non-stenotic carotid lesions with high-resolution MRI and ^{18}F -FDG PET imaging simultaneously using a combined PET/MRI system. In patients admitted for an ischaemic stroke considered as cryptogenic, we found in up to 40 % of the patients the presence of non-stenotic plaques with typical features of complicated plaques in the carotid artery ipsilateral to the stroke, supporting a causal role for these plaques in stroke. Accordingly, combined PET/MRI systems might find a role in the evaluation of patients admitted for an ischaemic stroke and presenting with non-stenotic carotid plaques.

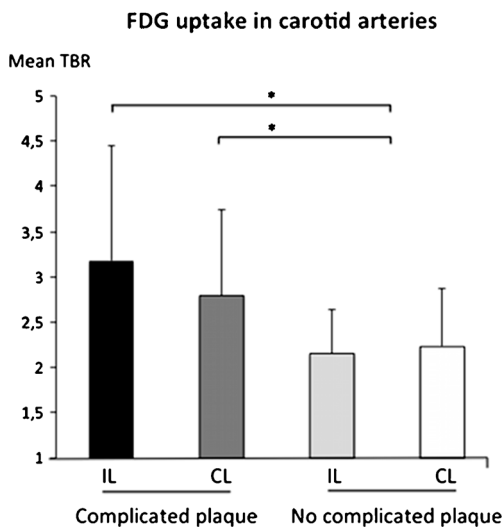


Fig. 4 Comparison of the intensity of ^{18}F -FDG uptake measured with PET in carotid arteries ipsilateral and contralateral to the territory of stroke in patients with or without complicated plaques with MRI. The highest ^{18}F -FDG uptake was detected in the carotid artery ipsilateral (IL) to the stroke in patients. ^{18}F -FDG uptake was also increased in the artery contralateral (CL) to the stroke in patients with complicated plaques in favour of a diffuse inflammatory process taking place in the vascular wall of these patients. * $p < 0.05$

Acknowledgments We thank Sylvia Schachoff, Anna Winter, and Claudia Meisinger for their valuable help in acquiring PET/MR images in the patients of this study and Isabelle Dregelly for setting up MRI sequences.

Ethical approval All procedures performed in studies involving human participants were in accordance with the ethical standards of the institutional and/or national research committee and with the 1964 Declaration of Helsinki and its later amendments or comparable ethical standards. The local Ethics Committee approved the study and all participants provided written informed consent.

Clinical Trial Registration: Unique Identifier NCT01284933; URL: <https://clinicaltrials.gov>

Funding sources This work was supported by the Advanced Research Grant “Multimodal Molecular Imaging” (MUMI; Grant number: 294582; European Research Council Executive Agency) and by the Deutsche Forschungsgemeinschaft (DFG; Grossgeräteinitiative).

Conflicts of interest Markus Schwaiger has a research cooperation contract with Siemens Healthcare AG. The other authors have no potential conflicts of interest relevant to this article.

References

- Go AS, Mozaffarian D, Roger VL, Benjamin EJ, Berry JD, Blaha MJ, et al. Heart disease and stroke statistics–2014 update: a report from the American Heart Association. *Circulation* 2014;129:e28–e292.
- Krishnamurthi RV, Feigin VL, Forouzanfar MH, Mensah GA, Connor M, Bennett DA, et al. Global and regional burden of first-ever ischaemic and haemorrhagic stroke during 1990–2010: findings from the Global Burden of Disease Study 2010. *Lancet Glob Health* 2013;1:e259–81.
- Bonita R. Epidemiology of stroke. *Lancet* 1992;339:342–4.
- Risk of stroke in the distribution of an asymptomatic carotid artery. The European Carotid Surgery Trialists Collaborative Group. *Lancet* 1995;345:209–12.
- Redgrave JN, Lovett JK, Gallagher PJ, Rothwell PM. Histological assessment of 526 symptomatic carotid plaques in relation to the nature and timing of ischemic symptoms: the Oxford plaque study. *Circulation* 2006;113:2320–8.
- Adams RJ, Albers G, Alberts MJ, Benavente O, Furie K, Goldstein LB, et al. Update to the AHA/ASA recommendations for the prevention of stroke in patients with stroke and transient ischemic attack. *Stroke* 2008;39:1647–52.
- Naghavi M, Libby P, Falk E, Casscells SW, Litovsky S, Rumberger J, et al. From vulnerable plaque to vulnerable patient: a call for new definitions and risk assessment strategies: Part II. *Circulation* 2003;108:1772–8.
- Rudd JH, Hyafil F, Fayad ZA. Inflammation imaging in atherosclerosis. *Arterioscler Thromb Vasc Biol* 2009;29:1009–16.
- Yuan C, Mitsumori LM, Beach KW, Maravilla KR. Carotid atherosclerotic plaque: noninvasive MR characterization and identification of vulnerable lesions. *Radiology* 2001;221:285–99.
- Yuan C, Mitsumori LM, Ferguson MS, Polissar NL, Echelard D, Ortiz G, et al. In vivo accuracy of multispectral magnetic resonance imaging for identifying lipid-rich necrotic cores and intraplaque hemorrhage in advanced human carotid plaques. *Circulation* 2001;104:2051–6.
- Tawakol A, Migrino RQ, Bashian GG, Bedri S, Vermylen D, Cury RC, et al. In vivo 18F-fluorodeoxyglucose positron emission tomography imaging provides a noninvasive measure of carotid plaque inflammation in patients. *J Am Coll Cardiol* 2006;48:1818–24.
- Rudd JH, Warburton EA, Fryer TD, Jones HA, Clark JC, Antoun N, et al. Imaging atherosclerotic plaque inflammation with [18F]-fluorodeoxyglucose positron emission tomography. *Circulation* 2002;105:2708–11.
- Judenhofer MS, Wehrl HF, Newport DF, Catana C, Siegel SB, Becker M, et al. Simultaneous PET-MRI: a new approach for functional and morphological imaging. *Nat Med* 2008;14:459–65.
- Rischpler C, Nekolla SG, Beer AJ. PET/MR imaging of atherosclerosis: initial experience and outlook. *Am J Nucl Med Mol Imaging* 2013;3:393–6.
- Amarenco P. Underlying pathology of stroke of unknown cause (cryptogenic stroke). *Cerebrovasc Dis* 2009;27 Suppl 1:97–103.
- Freilinger TM, Schindler A, Schmidt C, Grimm J, Cyran C, Schwarz F, et al. Prevalence of nonstenosing, complicated atherosclerotic plaques in cryptogenic stroke. *JACC Cardiovasc Imaging* 2012;5:397–405.
- Bayer-Karpinska A, Schwarz F, Wollenweber FA, Poppert H, Boeckh-Behrens T, Becker A, et al. The carotid plaque imaging in acute stroke (CAPIAS) study: protocol and initial baseline data. *BMC Neurol* 2013;13:201.
- Martinez-Möller A, Souvatzoglou M, Delso G, Bundschuh RA, Chefd'hotel C, Ziegler SI, et al. Tissue classification as a potential approach for attenuation correction in whole-body PET/MRI: evaluation with PET/CT data. *J Nucl Med* 2009;50:520–6.
- Delso G, Fürst S, Jakoby B, Ladebeck R, Ganter C, Nekolla SG, et al. Performance measurements of the Siemens mMR integrated whole-body PET/MR scanner. *J Nucl Med* 2011;52:1914–22.
- Schwaiger M, Ziegler SI, Nekolla SG. PET/CT challenge for the non-invasive diagnosis of coronary artery disease. *Eur J Radiol* 2010;73:494–503.
- Saam T, Raya JG, Cyran CC, Bochmann K, Meimarakis G, Dietrich O, et al. High resolution carotid black-blood 3T MR with parallel imaging and dedicated 4-channel surface coils. *J Cardiovasc Magn Reson* 2009;11:41.
- Hutton BF, Braun M, Thurjell L, Lau DY. Image registration: an essential tool for nuclear medicine. *Eur J Nucl Med Mol Imaging* 2002;29:559–77.
- Rosset A, Spadola L, Ratib O. OsiriX: an open-source software for navigating in multidimensional DICOM images. *J Digit Imaging* 2004;17:205–16.
- Rudd JH, Myers KS, Bansilal S, Machac J, Pinto CA, Tong C, et al. Atherosclerosis inflammation imaging with 18F-FDG PET: carotid, iliac, and femoral uptake reproducibility, quantification methods, and recommendations. *J Nucl Med* 2008;49:871–8.
- Cai JM, Hatsukami TS, Ferguson MS, Small R, Polissar NL, Yuan C. Classification of human carotid atherosclerotic lesions with in vivo multicontrast magnetic resonance imaging. *Circulation* 2002;106:1368–73.
- Kerwin W, Xu D, Liu F, Saam T, Underhill H, Takaya N, et al. Magnetic resonance imaging of carotid atherosclerosis: plaque analysis. *Top Magn Reson Imaging* 2007;18:371–8.
- Saam T, Ferguson MS, Yarnykh VL, Takaya N, Xu D, Polissar NL, et al. Quantitative evaluation of carotid plaque composition by in vivo MRI. *Arterioscler Thromb Vasc Biol* 2005;25:234–9.
- Kampschulte A, Ferguson MS, Kerwin WS, Polissar NL, Chu B, Saam T, et al. Differentiation of intraplaque versus juxtalumenal hemorrhage/thrombus in advanced human carotid atherosclerotic lesions by in vivo magnetic resonance imaging. *Circulation* 2004;110:3239–44.
- Hatsukami TS, Ross R, Polissar NL, Yuan C. Visualization of fibrous cap thickness and rupture in human atherosclerotic carotid plaque in vivo with high-resolution magnetic resonance imaging. *Circulation* 2000;102:959–64.
- Meyer BC, Hemmen TM, Jackson CM, Lyden PD. Modified National Institutes of Health Stroke Scale for use in stroke clinical trials: prospective reliability and validity. *Stroke* 2002;33:1261–6.
- Silvera SS, Aidi HE, Rudd JH, Mani V, Yang L, Farkouh M, et al. Multimodality imaging of atherosclerotic plaque activity and composition using FDG-PET/CT and MRI in carotid and femoral arteries. *Atherosclerosis* 2009;207:139–43.
- Saito H, Kuroda S, Hirata K, Magota K, Shiga T, Tamaki N, et al. Validity of dual MRI and F-FDG PET imaging in predicting

- vulnerable and inflamed carotid plaque. *Cerebrovasc Dis* 2013;35:370–7.
33. Figueroa AL, Subramanian SS, Cury RC, Truong QA, Gardecki JA, Tearney GJ, et al. Distribution of inflammation within carotid atherosclerotic plaques with high-risk morphological features: a comparison between positron emission tomography activity, plaque morphology, and histopathology. *Circ Cardiovasc Imaging* 2012;5:69–77.
 34. Tang TY, Howarth SP, Miller SR, Graves MJ, UKing-Im JM, Li ZY, et al. Comparison of the inflammatory burden of truly asymptomatic carotid atheroma with atherosclerotic plaques in patients with asymptomatic carotid stenosis undergoing coronary artery bypass grafting: an ultrasmall superparamagnetic iron oxide enhanced magnetic resonance study. *Eur J Vasc Endovasc Surg* 2008;35:392–8
 35. Kwee RM, Truijman MT, Mess WH, Teule GJ, ter Berg JW, Franke CL, et al. Potential of integrated [18F] fluorodeoxyglucose positron-emission tomography/CT in identifying vulnerable carotid plaques. *AJNR Am J Neuroradiol* 2011;32:950–4.
 36. Kwee RM, Teule GJ, van Oostenbrugge RJ, Mess WH, Prins MH, van der Geest RJ, et al. Multimodality imaging of carotid artery plaques: 18F-fluoro-2-deoxyglucose positron emission tomography, computed tomography, and magnetic resonance imaging. *Stroke* 2009;40:3718–24.
 37. Rominger A, Saam T, Wolpers S, Cyran CC, Schmidt M, Foerster S, et al. 18F-FDG PET/CT identifies patients at risk for future vascular events in an otherwise asymptomatic cohort with neoplastic disease. *J Nucl Med* 2009;50:1611–20.
 38. Marnane M, Prendeville S, McDonnell C, Noone I, Barry M, Crowe M, et al. Plaque inflammation and unstable morphology are associated with early stroke recurrence in symptomatic carotid stenosis. *Stroke* 2014;45:801–6.
 39. Marnane M, Merwick A, Sheehan OC, Hannon N, Foran P, Grant T, et al. Carotid plaque inflammation on 18F-fluorodeoxyglucose positron emission tomography predicts early stroke recurrence. *Ann Neurol* 2012;71:709–18.
 40. Huet P, Burg S, Le Guludec D, Hyafil F, Buvat I. Variability and uncertainty of 18F-FDG PET imaging protocols for assessing inflammation in atherosclerosis: suggestions for improvement. *J Nucl Med* 2015;56:552–9.
 41. Eldib M, Bini J, Robson PM, Calcagno C, Faul DD, Tsoumpas C, et al. Markerless attenuation correction for carotid MRI surface receiver coils in combined PET/MR imaging. *Phys Med Biol* 2015;60:4705–17.
 42. Bini J, Eldib M, Robson PM, Calcagno C, Fayad ZA. Simultaneous carotid PET/MR: feasibility and improvement of magnetic resonance-based attenuation correction. *Int J Cardiovasc Imaging* 2015